Computers and Geotechnics 119 (2020) 103381

Contents lists available at ScienceDirect

Computers and Geotechnics

journal homepage: www.elsevier.com/locate/compgeo

Research Paper

A comprehensive dissimilarity method of modeling accuracy evaluation for discontinuity disc models based on the sampling window

Jiongchao Wang[a], Jun Zheng[a,*], Tiexin Liu[b], Jichao Guo[a], Qing Lü[a]

[a] Department of Civil Engineering, Zhejiang University, Hangzhou 310058, China
[b] Highway and Bridge Engineering Institute, Dalian Maritime University, Dalian 116026, China

ARTICLE INFO

Keywords:
Discontinuity
Disc model
Modeling accuracy evaluation
Discrete fracture network (DFN)
Comprehensive dissimilarity
Rock mass

ABSTRACT

Discontinuity disc models are widely used to construct discrete fracture networks. It is important to evaluate the modeling accuracy and select the best network, which is most similar to the real rock mass, from multiple simulated networks. This study proposed a comprehensive dissimilarity method for modeling accuracy evaluation. The core of this method is the proposed index, comprehensive dissimilarity (*CD*), between the simulated model and the real rock mass, which is the average of the shape dissimilarity (*SD*), location dissimilarity (*LD*), and size dissimilarity (*ZD*). Some 3-D discontinuity networks were analyzed to validate the proposed comprehensive dissimilarity method. The results show that the method proposed in this paper is validated to quantitatively test the difference between the simulated models and real rock mass when multiple factors change at the same time. Finally, a rock slope at a hydropower station was used as a case study to illustrate the utility of the proposed method. The index *CD* comprehensively incorporates the orientation, location, size, and density of discontinuities and can be calculated by a computer code, the procedure of which is efficient and the results of which are objective. Therefore, the proposed method for evaluating the accuracy of models is worth popularizing.

1. Introduction

"Discontinuity" is a general and collective term for most types of joints, weak bedding planes, weak schistosity planes, zones of weakness, and faults [1]. Discontinuity patterns determine the deformation characteristics and stress-strain modes of a rock mass to a large extent and have a great influence on the stability and safety of rock engineering [2–4]. Therefore, it is necessary to quantitatively describe the discontinuities along with rock types in rock mass studies and engineering practices [1]. Unfortunately, in a real rock mass, most discontinuities are not visible, so it is impossible to measure all the discontinuities directly in three-dimensional (3-D) space [2]. To date, with respect to this problem, rock mass discontinuity network modeling has been applied to quantitatively represent discontinuities in 3-D space.

The core procedures of discontinuity network modeling are to select a discontinuity model and refer to the 3-D characteristics of discontinuities according to their 2-dimensional (2-D) or/and 1-dimensional (1-D) characteristics. The main discontinuity models include the disc model [5], similar parallelogram model [6], polygon model [7,8], and similar elliptical discs [9,10]. Due to mathematical convenience [9], among these models, the disc model is most widely used [2,11–15]. One of the key factors determining the success or failure of seepage, deformation, and stability analysis is whether the simulated discontinuity networks based on the disc model conform to the real rock mass. Therefore, it is particularly important to evaluate the modeling accuracy and select the best network, which is most similar to the real rock mass, from multiple simulated networks.

As stated above, most discontinuities are not directly observable in rock masses, so we have to perform modeling accuracy evaluation by comparing the dissimilarity of traces between real and simulated rock masses in the same sampling window (SW). The evaluation methods of modeling accuracy can mainly be divided into graphic testing and data testing. In terms of graphic testing, traditional methods rely on the observation of human eyes, which lack objectivity and hence have low accuracy and poor reliability. In recent years, many researchers have proposed new graphic testing methods by introducing the fractal dimension into this field [16–22]. However, the fractal dimension can only represent the degree of shape complexity of two graphs [23], and cannot reflect their similarities in position, size, and orientation. In terms of data testing, Baecher [24] and Vazaios [25] evaluated the reliability of the generated model by comparing the similarity between the cumulative length curve of traces of the real rock mass and

* Corresponding author.
E-mail address: zhengjun12@zju.edu.cn (J. Zheng).

https://doi.org/10.1016/j.compgeo.2019.103381
Received 18 September 2019; Received in revised form 1 November 2019; Accepted 1 December 2019
Available online 24 December 2019
0266-352X/

Nomenclature

A	feature point set [a_1, a_2, a_3, …, a_n] of the simulated trace map in the ith SW
B	feature point set [b_1, b_2, b_3,…, b_m] of the real trace map in the ith SW
BD_{si}	box-counting dimension of the simulated trace map in the ith SW
BD_{ri}	box-counting dimension of the real trace map in the ith SW
CD	comprehensive dissimilarity between the simulated and real trace maps
CD_{mean}	mean value of CD
d_{aibj}	distance between the ith point from A and the jth point from B
$d_{aib\min}$	minimum distance between the ith point from A and all the points from B
DD_i	directional dissimilarity between the simulated and real trace maps in the ith SW
ELD_i	extremity location dissimilarity between the real and simulated trace maps in the ith SW
$h_i(A, B)$	one-way HD from A to B
$h_i(B, A)$	one-way HD from B to A
HD	Hausdorff distance
$HD_i(A, B)$	the HD which is the maximum value of $h_i(A, B)$ and $h_i(B, A)$ between A and B in the ith SW
$HD_{i\max}$	the maximum HD between the simulated and real trace maps in the ith SW
HRD	half-feature point radius difference
HRD_{ij}	HRD of the jth circle of the ith SW
LD_i	location dissimilarity between the real and simulated trace map in the ith SW
LD	location dissimilarity between the simulated and real rock masses
MA_{si}	mean value of trace angles of the simulated trace map in the ith SW
MA_{ri}	mean value of trace angles of the real trace map in the ith SW
ML_{si}	mean value of trace lengths of the simulated trace map in the ith SW
ML_{ri}	mean value of trace lengths of the real trace map in the ith SW
OLD_i	overall location dissimilarity between the real and simulated trace maps in the ith SW
P_{30}	Discontinuity intensity, which means the number of discontinuities unit volume
R_{sij}	radius of the circle of which the centers are the jth point of the four endpoints and center point of the ith SW when the half-feature points of the simulated trace map are in the circle
R_{rij}	radius of the circle of which the centers are the jth point of the four endpoints and center point of the ith SW when the half-feature points of the real trace map are in the circle
RSD_i	relative shape dissimilarity between the real and simulated trace maps in the ith SW
SA_{si}	standard deviation of trace angles of the simulated trace map in the ith SW
SA_{ri}	standard deviation of trace angles of the real trace map in the ith SW
SD_i	shape dissimilarity between the real and simulated trace maps in the ith SW
SD	shape dissimilarity between the simulated and real rock masses
SDL_{si}	standard deviation of trace lengths of the simulated trace map in the ith SW
SDL_{ri}	standard deviation of trace lengths of the real trace map in the ith SW
SL_{si}	sum of trace lengths of the simulated trace map in the ith SW
SL_{ri}	sum of trace lengths of the real trace map in the ith SW
SW	sampling window
ZD_i	size dissimilarity between the real and simulated trace map in the ith SW
ZD	size dissimilarity between the simulated and real rock masses

simulated model. However, the method only considers the length distribution of traces and cannot reflect the characteristics of the trace positions and shapes. Moreover, due to considering a single factor (trace length), when the cumulative length curves of the traces of many models are very close to that of the original rock mass, it is difficult to judge which model is the best one. Han [26] evaluated the similarity between a simulated model and the real rock mass by comparing the statistical characteristic parameters of the trace lengths and orientations in the same SW between the real rock mass and the 125 simulated models. The method considers multiple parameters but fails to explain how to address the contradictory results of multiple parameters (e.g., the result of parameter A from Model 1 is better than that of Model 2, but the result of parameter B from Model 2 is better than that of Model 1; how should the optimum model be selected from these two models?).

With the development of noncontact measurement technologies (e.g., photogrammetry and laser scanning) for discontinuity geometries and the improvement of computer performance, it becomes increasingly easier to obtain a large number of measured geometric data of discontinuities and to generate network models. It is urgent that an objective and efficient evaluation method of modeling accuracy considering multiple factors is developed. This paper aims to propose an objective and efficient evaluation method for the discontinuity disc model by combining the knowledge of graphic similarity with traditional statistical methods.

2. Comprehensive dissimilarity method

As stated above, actual discontinuities are hidden in rock masses, so this study considers modeling accuracy evaluation by comparing the dissimilarity of traces between real and simulated rock masses in the same SW. For convenience of obtaining the traces, a local coordinate system is established, in which one endpoint of the rectangular SW is set as the origin and the long and short sides of the SW are set as the x-axis and y-axis, respectively. Based on the local coordinate system, one should obtain the following data: (a) the coordinates of the endpoints of the SW, (b) the number of traces, (c) the trace length, (d) the trace angle, and (e) the coordinates of the feature points of the traces.

The direction vector of a trace is defined as the vector that points to the endpoint with a larger y value from the endpoint with a smaller y value. The trace angle is defined as the angle of intersection between the direction vector of the trace and the positive x-axis, ranging from 0° to 180° (0° is included, but 180° is excluded). As shown in Fig. 1, θ_1 and θ_2 are the trace angles of traces 1 and 2, respectively.

The trace angle is used to represent the direction of the trace. However, a trace has two directions, so in some special situations, the trace angle defined above is problematic. As shown in Fig. 2, approximately parallel traces can be considered. The trace angles are labeled θ_i, and according to the figure, it is not difficult to obtain $\theta_1 = 18°$, $\theta_2 = 169°$, $\theta_3 = 165°$, $\theta_4 = 167°$, $\theta_5 = 172°$, and $\theta_6 = 162°$. Obviously, trace 1 is approximately parallel to the other five traces (Fig. 2); however, θ_1 is much smaller than the others. Therefore, the trace angles

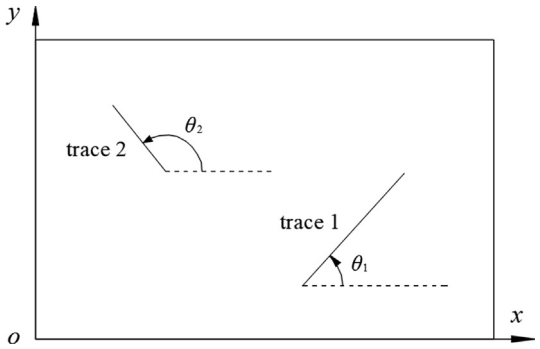

Fig. 1. Trace angles of traces 1 and 2.

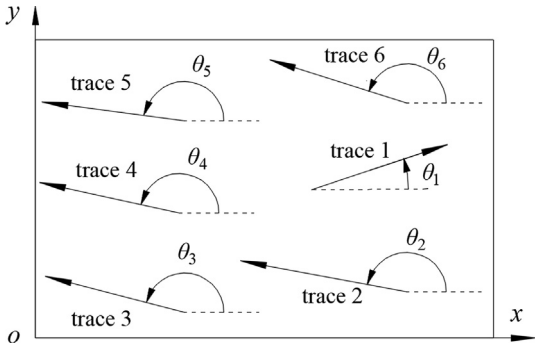

Fig. 2. An example of the identification of traces that need to be modified.

of the traces similar to trace 1 need to be modified. The modification procedure is as follows: (a) calculate the mean trace direction $\boldsymbol{n}_{\mathbf{m}}$ of all the traces; (b) with respect to a particular trace i, as shown in Fig. 3, if the angle of intersection between $\boldsymbol{n}_i$ and $\boldsymbol{n}_{\mathbf{m}}$ is larger than 90°, then the opposite direction is used as the modified trace direction, i.e., when the trace angle θ_i is larger than 90° (Fig. 3a), $\theta_i - 180°$ is used as the modified trace angle, and when the trace angle θ_i is smaller than 90° (Fig. 3b), $\theta_i + 180°$ is used as the modified trace angle.

For convenience, the traces need to be converted into a point set. Obviously, it is impossible to record all the points of the traces, and some feature points are chosen to represent the traces. The number of feature points for trace i is suggested to be $k_i + 2$, where k is an integer and is proportional to the length of the trace. The higher the number of feature points, the higher the accuracy, but the longer the calculation time. In this paper, k_i is equal to double trace length. All feature points of a trace are uniformly distributed along the trace. As shown in Fig. 4, it can be seen that the feature points can well reflect the basic characteristics of the traces. Once the trace data are obtained, one can start to evaluate the accuracy of the discontinuity disc model.

2.1. Shape dissimilarity

In recent years, fractal dimensions play an important role in the shape comparison of rock fracture networks [16–22]. Among these fractal dimensions, the box-counting dimension has been widely applied to measure the fractal dimension of natural fracture networks (Kulatilake et al. 1997). However, the box-counting dimension cannot test the difference in direction and location between two trace maps. As shown in Fig. 5, the two trace maps have the same box counting dimension, but they are completely different due to their divergent directions. Therefore, the box-counting dimension can only reflect the relative shape dissimilarity (RSD_i) between the simulated and real trace maps in the ith SW.

The direction of discontinuities has a great influence on the mechanical properties and permeability of the host rock masses. Therefore, it is necessary to add an indicator to evaluate the dissimilarity of the direction of traces between the simulated and real trace maps. In this paper, the mean value and standard deviation of the trace angles are selected for the indicator of directional dissimilarity (DD_i).

Therefore, the average value of RSD_i and DD_i is defined as the shape dissimilarity (SD_i) between the simulated and real trace maps in the ith SW. The following sections will discuss on RSD_i, DD_i, and SD_i in details.

2.1.1. Relative shape dissimilarity

As stated above, the box-counting dimension is used to evaluate the relative shape dissimilarity in this paper, and the calculation procedures are as follows [27].

(a) Assume that the size of the trace map is $b \times h$. Calculate all the common divisors between b and h, which are denoted d_1, d_2, d_3,..., and d_n, and divide the whole SW into square boxes with the side lengths of d_1, d_2, d_3,..., and d_n, respectively. When the side length of the square box is d_i, the total number of boxes is $(b \times h)/d_i^2$.
(b) Count the boxes containing feature points and record them as valid boxes. Denote the number of valid boxes as $N(d_i)$, and then a series of $(d_i, N(d_i))$ can be obtained.
(c) The series of $(d_i, N(d_i))$ are processed to obtain a series of $(-\log(d_i), \log(N(d_i)))$. Fit the series of $(-\log(d_i), \log(N(d_i)))$ by the least squares method to obtain a fitting line. The slope of the fitting line is the box-counting dimension of the trace map. It should be noted that the logarithmic processing is applied to d_i and $N(d_i)$ is based on the definition of the box-counting dimension as follows [28]

$$F = \lim_{d_i \to 0} \frac{N(d_i)}{-\log(d_i)} \tag{1}$$

where F is the box-counting dimension.

According to the above calculation method, the box-counting

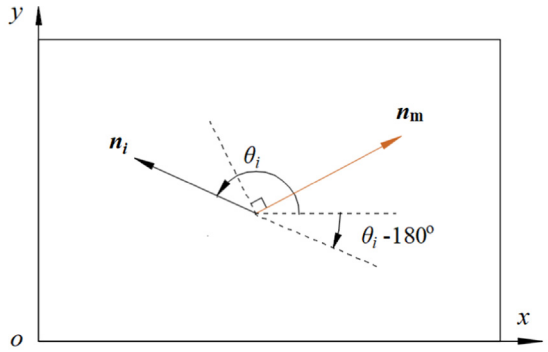

(a) $\theta_i > 90°$

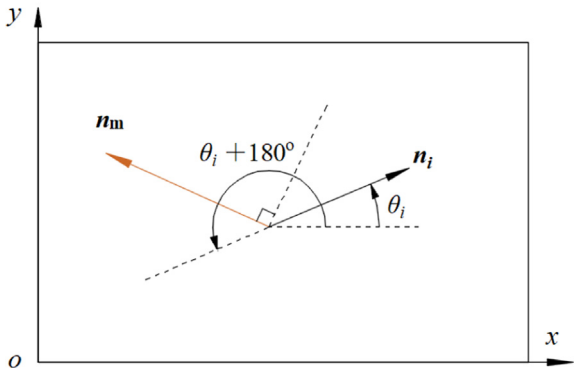

(b) $\theta_i < 90°$

Fig. 3. Modification of special trace angles.

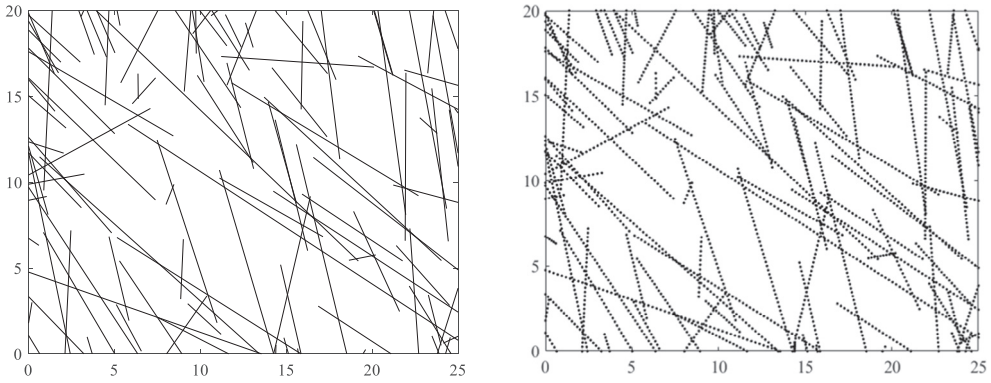

Fig. 4. Feature points of traces.

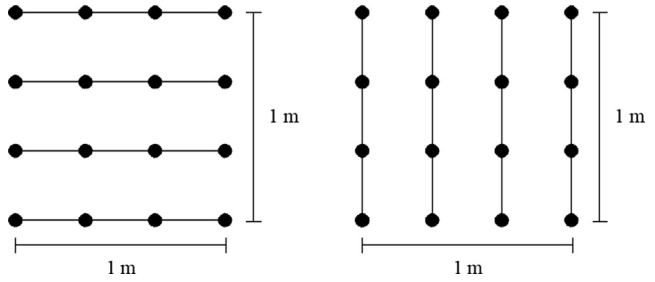

Fig. 5. An example showing that the box-counting dimension cannot reflect the difference in direction between two trace maps.

dimensions of the real and simulated trace maps in the *i*th SW can be calculated. Then, the RSD_i can be given by

$$RSD_i = \frac{|BD_{si} - BD_{ri}|}{BD_{ri}} \times 100\% \tag{2}$$

where BD_{si} and BD_{ri} are the box-counting dimension of the simulated and real trace maps, respectively.

2.1.2. Directional dissimilarity

First, calculate the mean value and standard deviation of the trace angles of each trace map. Then, the DD_i can be determined by

$$DD_i = \frac{\frac{|MA_{si} - MA_{ri}|}{MA_{ri}} + \frac{|SA_{si} - SA_{ri}|}{SA_{ri}}}{2} \times 100\% \tag{3}$$

where MA_{si} and SA_{si} are the mean value and standard deviation of the trace angles of the simulated trace map in the *i*th SW, respectively, and MA_{ri} and SA_{ri} are those of the real trace map. Note that when $|MA_i - MA_{ri}|$ is greater than 90°, in Eq. (3), $|MA_i - MA_{ri}|$ should be replaced by $180° - |MA_i - MA_{ri}|$.

Take the average of RSD_i and DD_i as the shape dissimilarity (SD_i), which is given by

$$SD_i = \frac{RSD_i + DD_i}{2} \tag{4}$$

The final directional dissimilarity between the simulated and real rock masses can be given by

$$SD = \frac{\sum_{i=1}^{n} SD_i}{n} \times 100\% \tag{5}$$

where n is the number of SWs.

2.2. Location dissimilarity

The shape dissimilarity is not sensitive to the locations of traces. As shown in Fig. 6, there are two trace sets with the same shape dissimilarity; however, they are different because of different locations. The Hausdorff distance (HD), which is widely used in image matching, facial recognition, computer vision and other fields [29–31], is introduced to represent the location dissimilarity. The HD is an index evaluating the maximum mismatch between two point sets and cannot reflect the overall location dissimilarity, so another index, called the half-feature point radius difference, is also developed (details explained below). Note that the dissimilarity obtained by the HD is called the extremity location dissimilarity.

2.2.1. Extremity location dissimilarity

Assume that the two feature point sets of the simulated and real

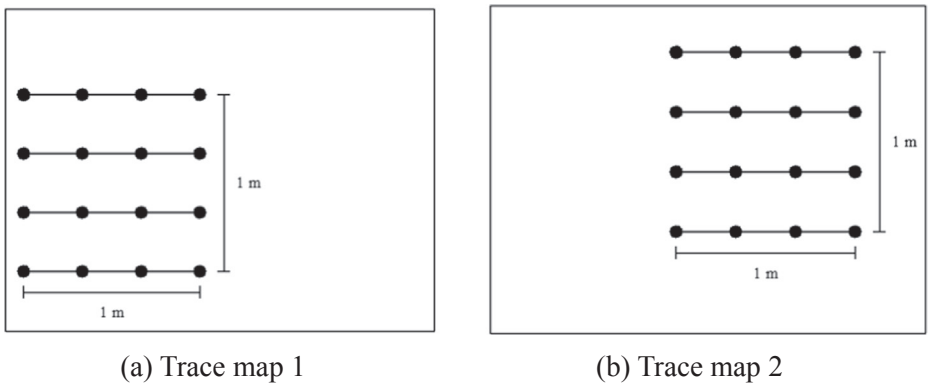

Fig. 6. An example showing that the shape dissimilarity cannot test the difference in location between two trace maps.

trace maps in the ith SW are $A = [a_1, a_2, a_3, \ldots, a_n]$ and $B = [b_1, b_2, b_3, \ldots, b_m]$. Thus, the Hausdorff distance between A and B is defined as [29–31]

$$HD_i(A, B) = \max(h_i(A, B), h_i(B, A)) \tag{6}$$

where $HD_i(A, B)$ is the HD between A and B, and $h_i(A, B)$ is called the one-way HD from A to B. $HD_i(A, B)$ is the maximum value of $h_i(A, B)$ and $h_i(B, A)$. The detailed procedures are as follows:

(a) For each a_i ($i = 1$ to n), calculate the distances d_{aibj} between a_i and b_j ($j = 1$ to m), and record the minimum distance d_{aibmin}, where the distance d_{aibj} can be given by

$$d_{aibj} = \sqrt{(x_i - x_j)^2 + (y_i - y_j)^2} \tag{7}$$

(b) Sort all d_{aibmin} and select the maximum value as $h_i(A, B)$.
(c) Apply the same procedures to get $h_i(B, A)$.
(d) Compare $h_i(A, B)$ with $h_i(B, A)$ and set the larger one to $HD_i(A, B)$.

The definition of the HD shows that the larger the value of HD is, the worse the position similarity of the two point sets. For each SW_i, the maximum HD (HD_{imax}) is the diagonal length of the rectangular SW. Therefore, the extremity location dissimilarity (ELD_i) is defined as

$$ELD_i = \frac{HD_i}{HD_{i\max}} \times 100\% \tag{8}$$

2.2.2. Overall location dissimilarity

As seen from the definition of HD, this index is susceptible to the influence of miscellaneous points. As shown in Fig. 7, the HD between the two trace maps is not equal to 0 because of the additional point in Fig. 7b.

To make up for this disadvantage of using the HD, an index called the half-feature point radius difference (HRD) is proposed to evaluate the difference in the overall distribution of traces. As shown in Fig. 8, five circles are drawn, centered at the four endpoints (O_{i1}, O_{i2}, O_{i3}, O_{i4}) and center point (O_{i5}) of the ith SW, and their radii are adjusted to let half of the feature points be in each circle. For the simulated trace map of the ith SW, the five radii are denoted R_{si1}, R_{si2}, R_{si3}, R_{si4} and R_{si5}, respectively; for the real trace map, the five radii are labeled R_{ri1}, R_{ri2}, R_{ri3}, R_{ri4} and R_{ri5}, respectively.

The HRD of the jth circle (HRD_{ij}) of the ith SW can be given by

$$HRD_{ij} = \frac{|R_{sij} - R_{rij}|}{R_{rij}} \times 100\% \tag{9}$$

where j is the serial number of the circles from to 1 to 5. The overall location dissimilarity (OLD_i) between the real and simulated trace maps in the ith SW is defined as

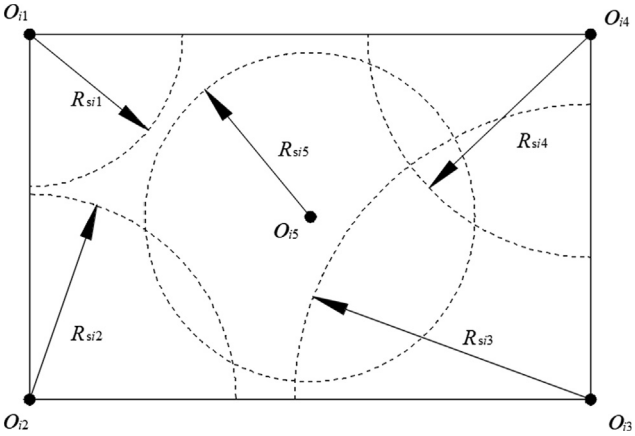

Fig. 8. An example of radii R_{si1}, R_{si2}, R_{si3}, R_{si4} and R_{si5} of the simulated trace map in the ith SW.

$$OLD_i = \frac{\sum_{j=1}^{5} HRD_{ij}}{5} \times 100\% \tag{10}$$

Take the average of ELD_i and OLD_i as the location dissimilarity (LD_i) between the real and simulated trace maps in the ith SW:

$$LD_i = \frac{ELD_i + OLD_i}{2} \tag{11}$$

The final location dissimilarity between the simulated and real rock masses can be given by

$$LD = \frac{\sum_{i=1}^{n} LD_i}{n} \times 100\% \tag{12}$$

where n is the number of SWs.

2.3. Size dissimilarity

The trace size is an important parameter of rock masses; however, the shape and location dissimilarities cannot accurately reflect the size characteristics. As shown in Fig. 9, the two trace maps have the same shape and location dissimilarities because of their same feature points, but the sizes of the traces are clearly different.

Three parameters, the sum, the mean and the standard deviation of the trace lengths, are selected to evaluate the size dissimilarity:

$$ZD_i = \frac{\frac{|SL_{si} - SL_{ri}|}{SL_{ri}} + \frac{|ML_{si} - ML_{ri}|}{ML_{ri}} + \frac{|SDL_{si} - SDL_{ri}|}{SDL_{ri}}}{3} \times 100\% \tag{13}$$

where SL_{si}, ML_{si}, and SDL_{si} are the sum, the mean and the standard

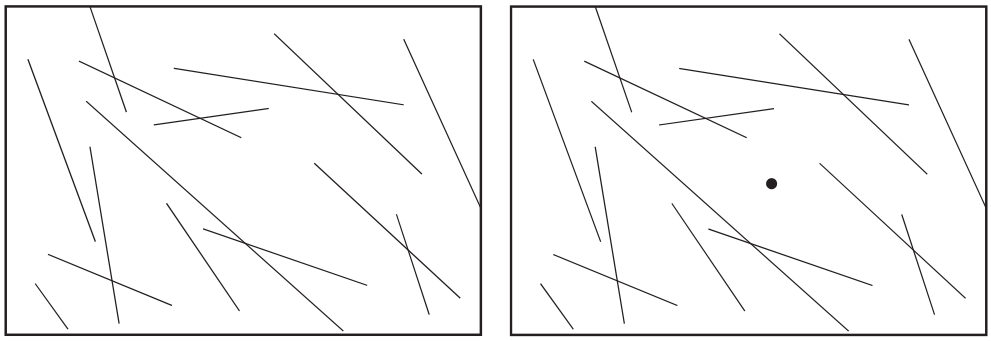

(a) Trace map 1 (b) Trace map 2

Fig. 7. An example showing the disadvantage of using the Hausdorff distance.

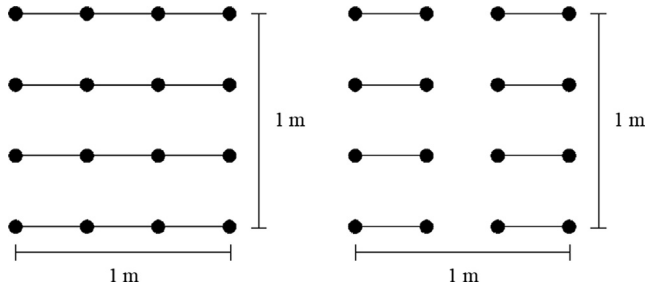

Fig. 9. An example showing that the shape and location dissimilarities cannot test the evaluation of trace lengths between two trace maps.

deviation of the trace lengths of the simulated trace map in the *i*th SW, respectively; and SL_{ri}, ML_{ri}, and SDL_{ri} are the sum, the mean and the standard deviation of the trace lengths of the real trace map in the *i*th SW, respectively.

$$ZD = \frac{\sum_{i=1}^{n} ZD_i}{n} \times 100\% \tag{14}$$

where n is the number of SWs.

2.4. Comprehensive dissimilarity

Take the average of *SD*, *LD*, and *ZD* as the comprehensive dissimilarity (*CD*) between the real and simulated trace maps; thus,

$$CD = \frac{SD + LD + ZD}{3} \times 100\% \tag{15}$$

When two trace maps are the same, *CD* is zero. Therefore, the lower the *CD* is, the closer the simulated model is to the real rock mass. In all, the calculation process of the comprehensive dissimilarity between two trace maps in one SW is given in Fig. 10. It should be noted that the acceptable value of *CD* is not fixed, and depends on the engineering purpose and the importance of the engineering, and *CD* is recommended to apply for judging which one of the generated models is most similar to the real rock mass.

3. Validation of the comprehensive dissimilarity method

Some 3-D discontinuity networks were constructed using Monte Carlo simulations, and the generated data were analyzed to validate the comprehensive dissimilarity method proposed in this study.

3.1. Construction of experimental models

First, we generated a discontinuity disc model as the real rock mass. In this model, the number of discontinuities is 3600. Discontinuities were assumed to be disc-shaped with gamma-distributed radii [32,33], uniformly distributed locations [14] and Fisher-distributed orientations for which the Fisher constant K is 25 [2]. The simulation volume was 30 m × 30 m × 30 m. To eliminate the influence of the boundary effect [26], the simulation volume was expanded by 3 m in the directions of x, $-x$, y, $-y$, z and $-z$. Therefore, the actual size of the simulation volume was 36 m × 36 m × 36 m. By combining the above discontinuity size, location, and orientation data, the real rock mass model was generated by Monte Carlo simulation. Note that to accentuate the dissimilarity, only one set of discontinuities is generated in this case.

By changing the parameters of the real rock mass, several models are generated to be compared with the real rock mass. Four model groups were generated, where the change ratios of parameters s were −10%, −20%, −30%, and −40%, respectively. For each group, three models were simulated, where the changed parameters include the mean dip angle of the discontinuities, the mean dip angle and mean radius of the discontinuities, and the mean dip angle, mean radius and number of the discontinuities (Table 1). Note that (a) the change ratio of a parameter is defined as (simulated value –real value)/(real value), e.g., for model 1-1, the ratio of mean dip angle = (40.5 − 45)/45 = −10%; and (b) the discontinuity numbers in Table 1 are determined by the simulation volume times the discontinuity intensity P_{30}, which means the number of discontinuities unit volume, and the change of discontinuity number represents the changes of P_{30}.

It can be clearly seen that for different model groups, the larger the change ratio is, the greater the difference between the model group and the real rock mass model. In the same model group, the model with a larger serial number is more divergent from the real rock mass model.

Two rectangular SWs (SW1 and SW2) are selected for measuring the

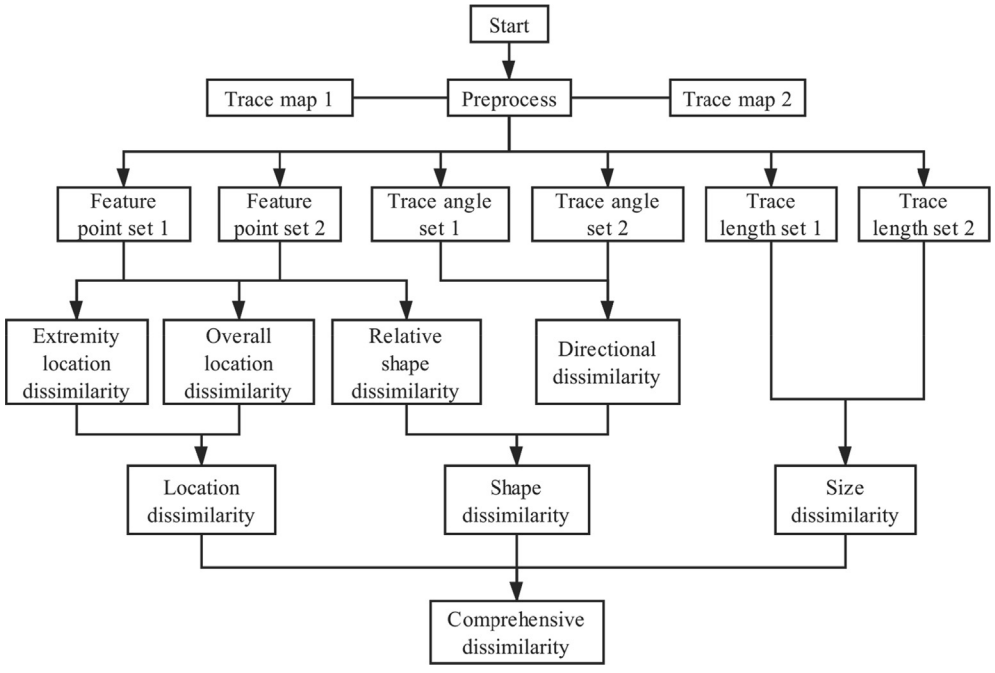

Fig. 10. The calculation process of the comprehensive dissimilarity between two trace maps in one SW.

Table 1
Parameters of the simulated and real models.

Model group #	Change ratio	Model #	Orientation				Radii		Discontinuity Number
			Distribution	*K*	Mean dip angle (°)	Mean dip direction (°)	Distribution	Mean value (m)	
0	0%	0	Fisher	25	45	180	Gamma	4	3600
1	10%	1-1			40.5			4	3600
		1-2			40.5			3.6	3600
		1-3			40.5			3.6	3240
2	20%	2-1			36			4	3600
		2-2			36			3.2	3600
		2-3			36			3.2	2880
3	30%	3-1			31.5			4	3600
		3-2			31.5			2.8	3600
		3-3			31.5			2.8	2520
4	40%	4-1			27			4	3600
		4-2			27			2.4	3600
		4-3			27			2.4	2160

Note: model group 0 represents the real rock mass.

traces of all the models. The dimensions of the two SWs are both 25 m × 20 m. Both center points of the two SWs are at (15, 15, 15). The dip direction and dip angle of SW1 are 140° and 40°, respectively, and the same parameters of SW2 are 320° and 50°, respectively. The short side of the SW is parallel to the projection of the line along the dip direction of the SW on the plane of the SW.

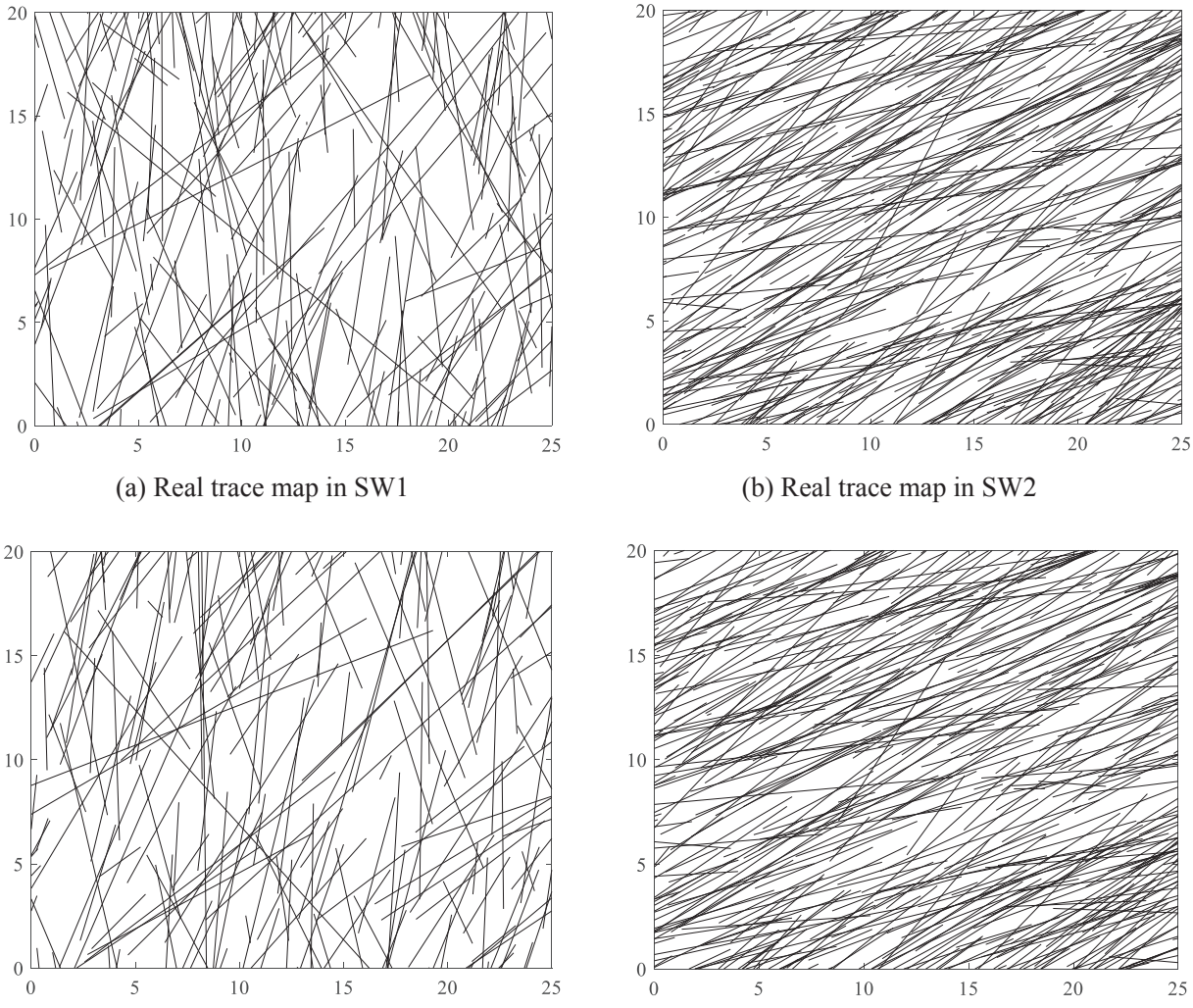

Fig. 11. The real and simulated trace maps.

3.2. Calculation procedures of CD

According to the comprehensive dissimilarity method proposed in this paper, the value of *CD* between each simulated model and the real rock mass model can be calculated. Take Model 1-1 as an example to demonstrate the calculation procedures of *CD*. The trace maps in two SWs of the real and simulated Model 1-1 rock masses are shown in Fig. 11.

(a) Measure the traces of the real and simulated rock masses in the aforementioned SWs (Fig. 10), and obtain the related parameters, as shown in Table 2.
(b) Calculate the shape dissimilarity: according to Fig. 10, BD_{s1} = 1.2589, BD_{r1} = 1.2873, and RSD_1 = 2.21% (Eq. (2)); according to Table 2, MA_{s1} = 75.29°, SA_{s1} = 24.10°, MA_{r1} = 83.76°, and SA_{r1} = 24.52°; according to Eqs. (3) and (4), DD_1 = 5.90% and SD_1 = 4.06%; similarly, SD_2 = 2.76%; and finally, SD = 3.41% (Eq. (5)).
(c) Calculate the location dissimilarity: according to Eqs. (6)–(8), HD_1 = 1.21, HD_{1max} = 32.02, ELD_1 = 3.80%; according to the feature point set 1 and 2, R_{s11} = 17.954, R_{s12} = 17.993, R_{s13} = 17.986, R_{s14} = 18.039, R_{s15} = 9.015, R_{r11} = 18.285, R_{r12} = 18.012, R_{r13} = 17.919, R_{r14} = 17.894, and R_{r15} = 9.341; according to Eqs. (10) and (11), OLD_1 = 1.32%, and LD_1 = 2.56%; similarly, LD_2 = 1.20%; and finally, LD = 1.88% (Eq. (12)).
(d) Calculate the size dissimilarity: according to the trace length data, SL_{s1} = 1202.7 m, ML_{s1} = 6.14 m, SDL_{s1} = 4.94 m, SL_{r1} = 1295.8 m, ML_{r1} = 5.84 m, and SDL_{r1} = 4.94 m; according to Eq. (13), ZD_1 = 4.14%; similarly, ZD_2 = 0.74%; and finally, ZD = 2.44% (Eq. (14)).
(e) Calculate the comprehensive dissimilarity: according to Eq. (15), CD = 2.58%.

The same procedures as above are used to calculate the values of CD of the other models.

3.3. Results

The values of *CD* between the experimental models and the real rock mass are given in Fig. 12. It should be noted that (Table 1) (a) as the model group number increases from 1 to 4, the change ratio of the parameters of the simulated models increases from 10% to 40%, i.e., the difference between the simulated and real rock masses increases as the model group number increases; and (b) for models with the same group number, as the model number increases from 1 to 3, the number of changed parameters increases from 1 to 3, i.e., the difference between the simulated and real rock masses increases as the model number increases when their model group numbers are the same. The results of Fig. 12 show that (a) for the same model group, the value of *CD* of the model with a smaller model number is lower, which conforms to the reality of the models; and (b) as the model group number increases, the value of *CD* increases, which well reflects the difference in models from the same model group; therefore, (c) the method proposed in this paper is validated to quantitatively test the difference between the simulated and real rock mass models when multiple factors change at the same time.

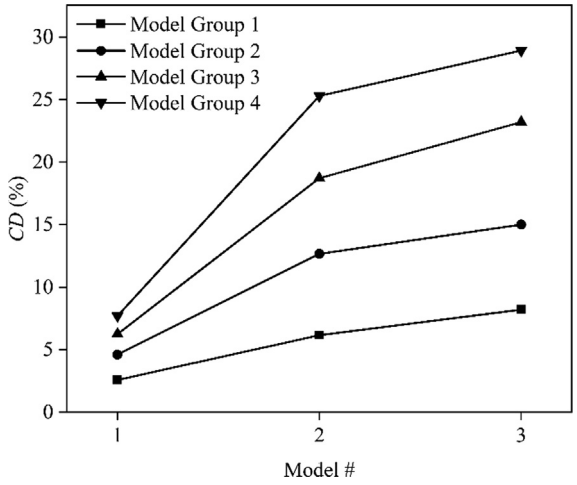

Fig. 12. The experimental results.

To estimate the influence of changed parameters on the values of *SD*, *LD*, and *ZD*, the results of Model Group 4 are further analyzed. Note that (a) Model Group 4 in the above experiment has the largest changes; (b) according to Table 1, compared to the real rock mass, the mean dip angle of the discontinuities changes by 40% for Model 4-1; (c) the mean dip angle and mean radius of the discontinuities change by 40% for Model 4-2; and (d) the mean dip angle, mean radius and number of the discontinuities change by 40% for Model 4-3. Because the model with a larger model number is obtained by adding a changed parameter based on the model with a smaller number, the relative values of *SD*, *LD*, and *ZD* can be calculated to estimate the influence of the changed parameters on the values of the three indexes. The computations and results of the relative values of *SD*, *LD*, and *ZD* are given in Table 3.

Table 3 shows the following: (a) 40% changes in the orientation, radius, and number of discontinuities produce *SD* values of 17.10%, 11.58%, and 3.96%, respectively; thus, *SD* mainly reflects the dissimilarity of orientation and radius, especially orientation; (b) the same changes produce *LD* values of 1.92%, 1.24%, and 2.55%, respectively, all of which are small because the locations of the discontinuities in the real and simulated models both follow uniform distributions; thus, *LD* mainly reflects the dissimilarity of location and is not sensitive to the orientation, radius, and number of discontinuities; (c) the same changes produce *ZD* values of 4.07%, 39.99%, and 4.4%, respectively; thus, *ZD* mainly reflects the dissimilarity of radius; (d) the above conclusions are

Table 2
Calculated parameters based on the trace maps (Model 1-1).

SW #	Parameters	Name of statistical indexes	The real rock mass model	The no.1 model of the no.1 model group
SW1	Feature point set		Feature point set 1	Feature point set 2
	Trace angle	Mean value	83.76°	75.29°
		Standard deviation	24.52°	24.10°
	Trace length	Mean value	5.84 m	6.13 m
		Standard deviation	4.94 m	4.94 m
		Sum	1295.8 m	1202.7 m
SW2	Feature point set		Feature point set 3	Feature point set 4
	Trace angle	Mean value	29.05°	26.68°
		Standard deviation	18.16°	17.90°
	Trace length	Mean value	6.48 m	6.60 m
		Standard deviation	4.75 m	4.43 m
		Sum	2778.5 m	2771.7 m

Table 3
The relative values of *LD*, *SD*, and *ZD* between Model Group 4 and the real rock masses.

Model #	Index			Represented properties of discontinuities
	Name	Value (%)	Relative value (%)	
4-1	*SD*	17.10	17.10 − 0 = 17.10	Orientation
4-2		28.68	28.68 − 17.10 = 11.58	Radius
4-3		32.64	32.64 − 28.68 = 3.96	Number
4-1	*LD*	1.92	1.92 − 0 = 1.92	Orientation
4-2		3.16	3.16 − 1.92 = 1.24	Radius
4-3		5.71	5.71 − 3.16 = 2.55	Number
4-1	*ZD*	4.07	4.07 − 0 = 4.07	Orientation
4-2		44.06	44.06 − 4.07 = 39.99	Radius
4-3		48.46	48.46 − 44.06 = 4.4	Number

consistent with the definition of *SD*, *LD*, and *ZD*; and (e) according to the large relative values of *SD*, *LD*, and *ZD*, one may consider adjusting the corresponding discontinuity parameter(s).

4. Engineering application

The Changhe dam is a rockfill dam in Sichuan Province, China, and its water release system consists of three diversion tunnels, one releasing tunnel, and three spillway tunnels. Liu et al. [34] used a 3-D photographic measurement system to measure traces in four SWs on the tunnel slope of spillway No. 3. The slope consists mainly of medium-coarse grained granite and quartz diorite and is made up of two perpendicular sections. The dip directions of the two sections are approximately 283° and 13°. The dip angle of this slope ranges from 78° to 84°, and the height of the slope is 500–600 m. Due to the multistage tectonic movement in this area, the discontinuities are well developed in the slope rock mass, and there is no filling in these discontinuities [34] (see Fig. 13).

The fourth SW introduced by Liu [34] is used as an example in this study. The dip direction and dip angle of the SW are 102.6° and 83.1°, respectively, and the size is 30 m × 10 m. The discontinuities are divided into three sets based on their orientations [34]. Because there are very few traces in the upper and lower areas of the fourth SW, it is not suitable to take the whole SW as the research object. Therefore, the area where the *y* coordinate ranges from 2 to 9 in the SW is selected as the studied SW, i.e., the size of the SW of the real trace map is 30 m × 7 m (red window in Fig. 14a).

Based on the sampled geometric parameters of the discontinuities (Table 4), five discontinuity disc models with dimensions of 30 m × 30 m × 10 m are constructed by Monte Carlo simulation. It should be noted that the sizes of the discontinuities are obtained by the analytical method for estimating the diameter distribution proposed by Zhang et al. [35], the locations obey the uniform distribution, and the orientations obey the Fisher distribution. The related parameters for constructing five discontinuity disc models are given in Table 4 and Fig. 15.

The SW with the same orientation as the fourth SW in the tunnel slope of spillway No. 3 is used, and then the simulated trace maps of the five models can be obtained. It should be noted that since it is

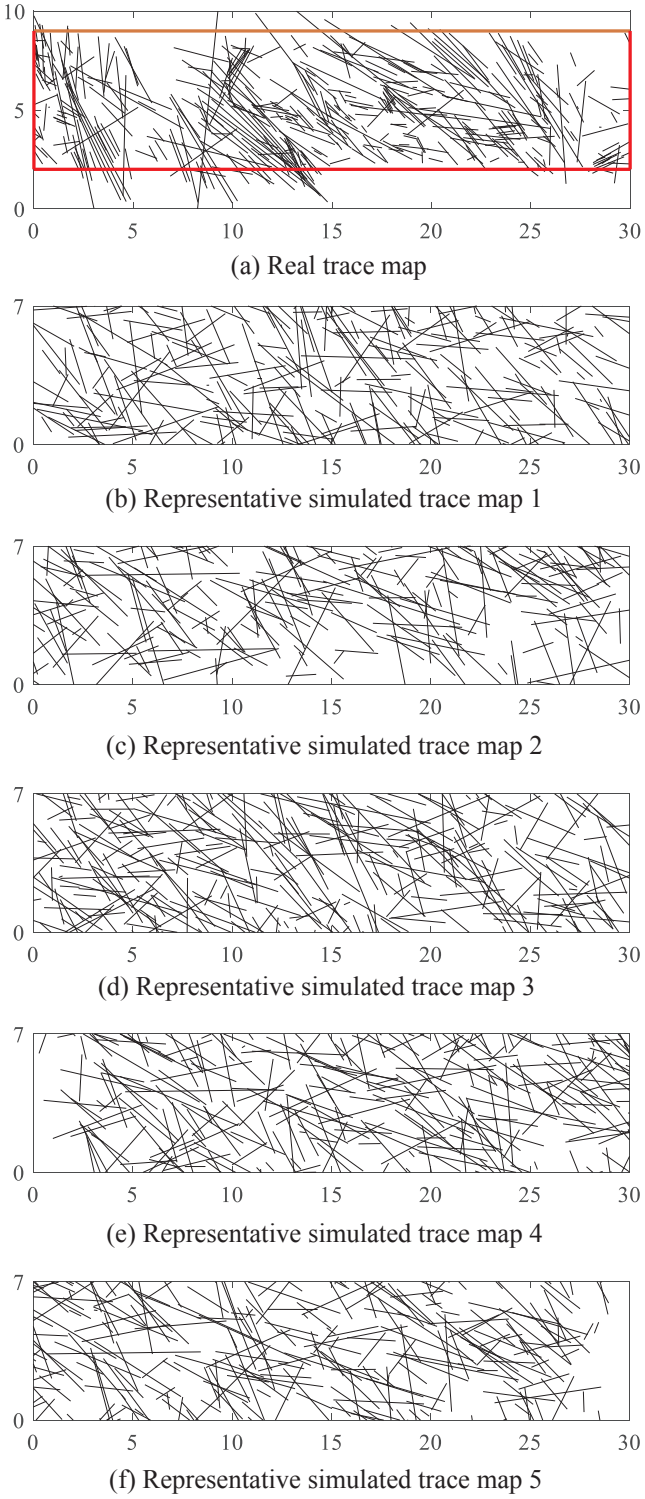

Fig. 14. Real and five representative simulated trace maps.

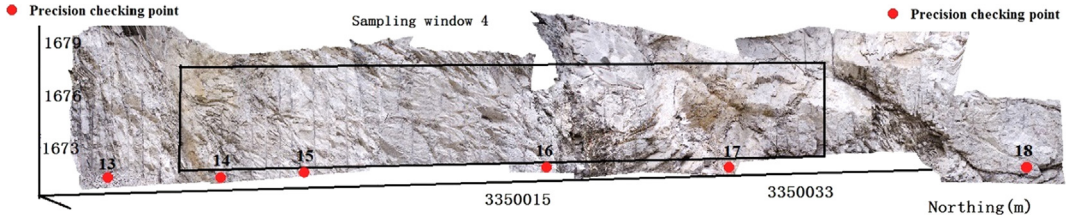

Fig. 13. The fourth SW in the tunnel slope of spillway No. 3 [34].

Table 4
Parameters for constructing five discontinuity disc models.

Discontinuity set #	Discontinuity orientations			Intensity P_{30} (m^{-3})
	Mean dip angle (°)	Mean dip direction (°)	Fisher constant K	
1	62.98	34.02	3.76	0.12
2	60.36	300.10	6.35	0.22
3	33.37	97.23	2.59	0.20

Table 5
Four dissimilarities between the five simulated models and the real rock mass.

Model #	*SD*	*LD*	*ZD*	*CD*
1	9.79%	4.63%	18.87%	11.10%
2	14.41%	4.98%	24.45%	14.61%
3	8.99%	4.29%	18.27%	10.52%
4	10.10%	4.99%	20.45%	11.85%
5	9.37%	7.52%	19.15%	12.02%

impossible to know the specific position of the SW in the model, the sampling windows with the five center points of (15,15,5), (15,15,3), (15,15,7) (15,13,5), and (15,17,5) are selected to sample traces in each model five times. Calculate *CD* between the five simulated trace maps of each model and the real trace map and take the mean value of the five *CD*s as the final *CD* between the model and real rock mass (see Table 5).

The values of final *CD* are 11.10%, 14.61%, 10.52%, 11.85%, and 12.02% for the five simulated models. Among them, the *CD* of Model 3 is the minimum, which is 10.52%, so Model 3 is selected as the best model. With respect to Model 3, the values of *SD*, *LD*, and *ZD* are 4.29%, 8.99%, and 18.27%, respectively, which implies that the estimation and simulation of the size of discontinuities has further room for improvement.

In addition, it should be noted that it is difficult to determine which trace map is most similar to the real trace map by the direct observation, as shown in Fig. 14b to f, but the CD values of trace maps are a good quantitative and objective index for evaluating the accuracy of models considering multiple factors. Therefore, the proposed method for evaluating model accuracy is worth popularizing.

5. Summary and conclusions

In this paper, a comprehensive dissimilarity method of modeling accuracy evaluation for discontinuity disc models was developed. The core of this method was to propose a comprehensive index, *CD*, between the simulated model and the real rock mass; *CD* is the average value of *SD*, *LD*, and *ZD*. A lower value of *CD* indicates a smaller difference between the simulated model and the real rock mass.

Some 3-D discontinuity networks were constructed using Monte Carlo simulations, and the generated data were analyzed to validate the proposed comprehensive dissimilarity method. The results show that (a) for the same model group, the value of *CD* of the model with a smaller model number is lower, which conforms to the reality of the models; and (b) as the model group number increases, the value of *CD* increases, which well reflects the difference in models from the same model group; therefore, (c) the method proposed in this paper is validated to quantitatively test the difference between the simulated and real rock mass models when multiple factors change at the same time. In addition, *LD*, *SD,* and *ZD* are also independently analyzed, and some conclusions are drawn: (a) *SD* mainly reflects the dissimilarity of orientation and radius, especially orientation; (b) *LD* mainly reflects the dissimilarity of location, and are not sensitive to orientation, radius, and number of discontinuities; (c) *ZD* mainly reflects the dissimilarity of radius; (d) therefore, according to the large relative values of *SD*, *LD*, or *ZD*, one may consider adjusting the corresponding parameter(s) of discontinuities.

A rock slope at a hydropower station in China was used as a case study to illustrate the use of the proposed method. Based on the sampled geometric parameters of the discontinuities, five discontinuity disc models were constructed The values of *CD* are 11.10%, 14.61%, 10.52%, 11.85%, and 12.02% for the five simulated models. Among them, the *CD* of Model 3 is the minimum, which is 10.52%, so Model 3 is selected as the best model. With respect to Model 3, the values of *SD*, *LD*, and *ZD* are 4.29%, 8.99%, and 18.27%, respectively, which implies that the estimation and simulation of the size of discontinuities has the maximum room for improvement. In addition, the case study clearly showed the superiority of the comprehensive dissimilarity method over graphic comparison by the direct observation.

The index *CD* comprehensively incorporates the orientation, location, size, and density of discontinuities and can be calculated by a computer code, the procedure of which is efficient and the results of which are objective. Therefore, this proposed method for evaluating the accuracy of models is worth popularizing.

CRediT authorship contribution statement

Jun Zheng: Conceptualization, Funding acquisition, Investigation, Writing - review & editing. **Jiongchao Wang:** Methodology, Data curation, Formal analysis, Writing - original draft. **Tiexin Liu:** Validation, Resources. **Jichao Guo:** Visualization. **Qing Lü:** Writing - review & editing.

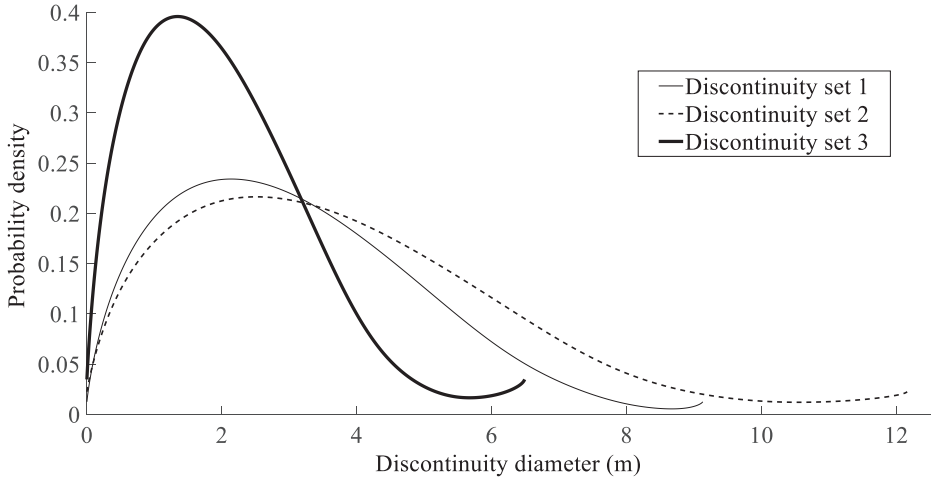

Fig. 15. Probability density function of discontinuity diameters of three sets.

Declaration of Competing Interest

The authors declare that they have no known competing financial interests or personal relationships that could have appeared to influence the work reported in this paper.

Acknowledgments

This study was funded by the National Key R&D Program of China (2018YFC1505005), the Fundamental Research Funds for the Central Universities (3132018120), the National Natural Science Foundation Projects (41972264 & 41772287), and the Natural Science Foundation of Zhejiang Province, China (LY18E090002).

References

[1] ISRM. International society for rock mechanics commission on standardization of laboratory and field tests: Suggested methods for the quantitative description of discontinuities in rock masses. Int J Rock Mech Min Sci Geomech Abstr 1978;15(6):319–68.
[2] Zheng J, Deng J, Yang X, Wei J, Zheng H, Cui Y. An improved Monte Carlo simulation method for discontinuity orientations based on Fisher distribution and its program implementation. Comput Geotech 2014;61(3):266–76.
[3] Fan X, Li K, Lai H, Xie Y, Cao R, Zheng J. Internal stress distribution and cracking around flaws and openings of rock block under uniaxial compression: a particle mechanics approach. Comput Geotech 2018;102:28–38.
[4] Jiang Q, Yan F, Wu J, Fan Q, Li S, Xu D. Grading opening and shearing deformation of deep outward-dip shear belts inside high slope: a case study. Eng Geol 2019;250:113–29.
[5] Baecher GB, Lanney NS, Einstein HH. Statistical descriptions of rock properties and sampling. In: Proceedings of the 18th U.S. symposium on rock mechanics, (5C1-1–5C1-8); 1977.
[6] Warburton PM. Stereological interpretation of joint trace data: Influence of joint shape and implications for geological surveys. Int J Rock Mech Min Sci Geomech Abstr 1980;17(6):305–16.
[7] Ivanova V. Geologic and stochastic modeling of fracture systems in rocks Ph D thesis Cambridge: Massachusetts Institute of Technology; 1998. p. 530.
[8] Meyer T. Geologic stochastic modeling of rock fracture systems related to crustal faults Ph D thesis Cambridge: Massachusetts Institute of Technology; 1999. p. 406.
[9] Zhang L, Einstein HH, Dershowitz WS. Stereological relationship between trace length and size distribution of elliptical discontinuities. Géotechnique 2002;52(6):419–33.
[10] Jin W, Gao M, Zhang R, Zhang G. Analytical expressions for the size distribution function of elliptical joints. Int J Rock Mech Min Sci 2014;70:201–11.
[11] Kulatilake PHSW. Application of probability and statistics in joint network modeling in three dimensions. Proceedings of the Conference on Probabilistic Methods in Geotechnical Engineering, Canberra, Australia. 1993. p. 63–87.
[12] Zhang L, Einstein HH. Estimating the mean trace length of rock discontinuities. Rock Mech Rock Eng 1998;31(4):217–35.
[13] Priest SD. Determination of discontinuity size distributions from scanline data. Rock Mech Rock Eng 2004;37(5):347–68.
[14] Zheng J, Deng J, Zhang G, Yang X. Validation of Monte Carlo simulation for discontinuity locations in space. Comput Geotech 2015;67:103–9.
[15] Xiong F, Jiang Q, Xu C, Zhang X, Zhang Q. Influences of connectivity and conductivity on nonlinear flow behaviours through three-dimension discrete fracture networks. Comput Geotech 2019;107:128–41.
[16] Bagde MN, Raina AK, Chakraborty AK, Jethwa JL. Rock mass characterization by fractal dimension. Eng Geol 2002;63(1):141–55.
[17] Pourghasemi HR, Moradi HR, Aghda SMF, Sezer EA, Jirandeh G, Pradhan BP. Assessment of fractal dimension and geometrical characteristics of the landslides identified in North of Tehran. Iran Environ Earth Sci 2014;71(8):3617–26.
[18] Liu R, Li B, Jiang Y. A fractal model based on a new governing equation of fluid flow in fractures for characterizing hydraulic properties of rock fracture networks. Comput Geotech 2016;75:57–68.
[19] Zhao Y, Feng Z, Yang D, Liang W, Feng Z. Three-dimensional fractal distribution of the number of rock-mass fracture surfaces and its simulation technology. Comput Geotech 2015;65:136–46.
[20] Jörn HK. Fractal-geometry techniques in the quantification of complex rock structures: a special view on scaling regimes, inhomogeneity, and anisotropy. J Struct Geol 2013;46(46):2–21.
[21] Kulatilake PHSW, Fiedler R, Panda BB. Box fractal dimension as a measure of statistical homogeneity of jointed rock masses. Eng Geol 1997;48:217–29.
[22] Odling NE. Natural fracture profiles, fractal dimension and joint roughness coefficients. Rock Mech Rock Eng 1994;27(3):135–53.
[23] Backes AR, Bruno OM. A new approach to estimate fractal dimension of texture images. Image Signal Process 2008:136–43.
[24] Baecher GB. Statistical analysis of rock mass fracturing. Math Geol 1983;15(2):329–48.
[25] Vazaios I, Farahmand K, Vlachopoulos N, Diederichs MS. Effects of confinement on rock mass modulus: A synthetic rock mass modelling (SRM) study. Int J Rock Mech Min 2018;10(3):436–56.
[26] Han XD, Chen JP, Wang Q, Li YY, Zhang W, Yu TW. A 3D fracture network model for the undisturbed rock mass at the Songta Dam site based on small samples. Rock Mech Rock Eng 2016;49(2):611–9.
[27] Khotimah C, Juniati D. Iris recognition using feature extraction of box counting fractal dimension. J Phys Conf Ser 2018;947(1):1–6.
[28] Falconer K. Fractal geometry: mathematical foundations and applications. 2nd ed., Chichester: John Wiley & Sons; 2004.
[29] Jesorsky O, Kirchberg KJ, Frishholz RW. Robust face detection using the Hausdorff distance. AVBPA. 2001. p. 90–5.
[30] Huttenlocher DP, Klanderman GA, Rucklidge WJ. Comparing images using the Hausdorff distance. IEEE T Pattern Anal 1993;15(9):850–63.
[31] Weng H, Wang S, Lin X, Li Z, Huang J. A novel criterion applicable to transformer differential protection based on waveform sinusoidal similarity identification. Int J Elec Power 2019;105:305–14.
[32] Zhang L, Einstein HH. Estimating the intensity of rock discontinuities. Int J Rock Mech Min Sci 2003;37(5):819–37.
[33] Kulatilake PHSW, Um JG, Wang M, Escandon RF, Narvaiz J. Stochastic fracture geometry modeling in 3-D including validations for a part of Arrowhead East Tunnel, California, USA. Eng Geol 2003;70(1):131–55.
[34] Liu T, Deng J, Zheng J, Zheng L, Zhang Z, Zheng H. A new semi-deterministic block theory method with digital photogrammetry for stability analysis of a high rock slope in China. Eng Geol 2017;216:76–89.
[35] Zhang G, Fei W, Zhang R, Deng J. Analytical method for inferring the diameter distribution of joint poisson disk model. Rock Soil Mech 2011;4:1149–56. [in Chinese].